Cavity ring-down spectroscopy and theoretical calculations of the $S_1(^1B_{3u}) \leftarrow S_0(^1A_g)$ transition of jet-cooled perylene

Xiaofeng Tan[a] and Farid Salama[b]
Space Science Division, NASA Ames Research Center, Mail Stop 245-6, Moffett Field, California 94035-1000

(Received 26 October 2004; accepted 3 December 2004; published online 18 February 2005)

As part of our long-term program to test the diffuse interstellar band–polycyclic aromatic hydrocarbon hypothesis, we have investigated the $S_1 \leftarrow S_0$ electronic transition of neutral perylene ($C_{20}H_{12}$) in a combined experimental and theoretical study. Jet-cooled perylene was prepared with a pulsed discharge slit nozzle and detected by cavity ring-down spectroscopy. A number of vibronic features were observed in the 24 000–24 900 cm^{-1} spectral range. Density functional and *ab initio* calculations were performed to determine the geometries, harmonic vibrational frequencies, and normal coordinates of both the S_0 and S_1 electronic states. A rotational temperature of 52 ± 5 K was derived from a rotational contour analysis of the vibronic band associated with the 0-0 transition. A Franck–Condon treatment was carried out to calculate the vibronic spectrum of the $S_1 \leftarrow S_0$ transition. A good agreement was found between the calculated and the experimental spectra. A vibrational assignment is proposed and six normal modes are identified. The contribution of neutral compact polycyclic aromatic hydrocarbons to the diffuse interstellar bands is briefly discussed.
 [DOI: 10.1063/1.1851502]

I. INTRODUCTION

Polycyclic aromatic hydrocarbons (PAHs) have been suggested to be the possible molecular carriers of the ubiquitous diffuse interstellar bands (DIBs) seen in absorption in the spectra of stars obscured by diffuse interstellar clouds.[1–6] Despite the fact that DIBs were first discovered in 1922,[7] there is no firm identification of the cariers of these bands. Extensive laboratory efforts have been devoted to assess the validity of this proposal by measuring the electronic spectra of various neutral and ionized PAHs under conditions that mimic those found in the interstellar clouds where the DIBs are originated.[8] Earlier experimental data were primarily obtained with matrix-isolation spectroscopy (MIS) due to its capability of trapping neutral and ionized PAHs in cryogenic inert-gas solid matrices.[9,10] The spectral features recorded with MIS, however, are shifted and broadened due to the interaction of the trapped species with the solid lattice. This shortcoming was overcome by the application of cavity ring-down spectroscopy (CRDS).[11–13] Only a limited number of PAHs have been studied by CRDS due to the difficulty of bringing these low-vapor pressure molecules into the gas phase in amounts detectable under the laboratory conditions that are relevant for astrophysical studies.[14–18]

We select the $S_1(^1B_{3u}) \leftarrow S_0(^1A_g)$ transition of neutral perylene because it can be served as a model system for the study of middle-size compact PAHs of similar structure. The absorption spectra of both neutral and ionized perylene have been measured with MIS.[19–24] Perylene has been noted for its remarkable intramolecular vibrational redistribution (IVR) effects in the S_1 state. Laser-induced fluorescence (LIF) experiments have shown that low vibrational states ($E_{vib} < 700$ cm^{-1}) in the S_1 state show no observable IVR on the time scale of emission while high vibrational states ($E_{vib} > 1600$ cm^{-1}) in the S_1 state show very fast IVR.[25–27] A model of anharmonic coupling has been proposed to explain the observed results.[26] The vibrational frequencies in the S_0 state are available from earlier theoretical calculations.[28,29] The calculated frequencies, however, were found to be in poor agreement with the experimental values. The vibrational frequencies of the IR-active modes in the S_0 state were also reported.[30] To the best of our knowledge, theoretical vibrational frequencies in the S_1 state have not been reported.

In the present paper, we present the cavity ring-down spectrum of the $S_1 \leftarrow S_0$ electronic transition of jet-cooled neutral perylene ($C_{20}H_{12}$) in the 24 000–24 900 cm^{-1} (401.6–416.7 nm) spectral range. Quantum chemical calculations are carried out to determine the equilibrium geometries, harmonic vibrational frequencies, and normal coordinates in both the S_0 and S_1 electronic states. A rotational contour analysis is performed to derive the rotational temperature. Finally, a Franck–Condon treatment is carried out to calculate the vibronic spectrum of the $S_1 \leftarrow S_0$ transition. A vibrational assignment for the observed spectral features is proposed, and six normal modes are identified in the observed spectrum.

II. EXPERIMENT

A. Apparatus

The experimental apparatus has been described in detail previously.[15,16] A pulsed supersonic beam containing gas mixtures of neutral perylene (Sigma-Aldrich, purity >99%) and Ar was prepared with a pulsed discharge slit nozzle

[a]Electronic mail: x.tan@jhu.edu
[b]Electronic mail: Farid.Salama@nasa.gov

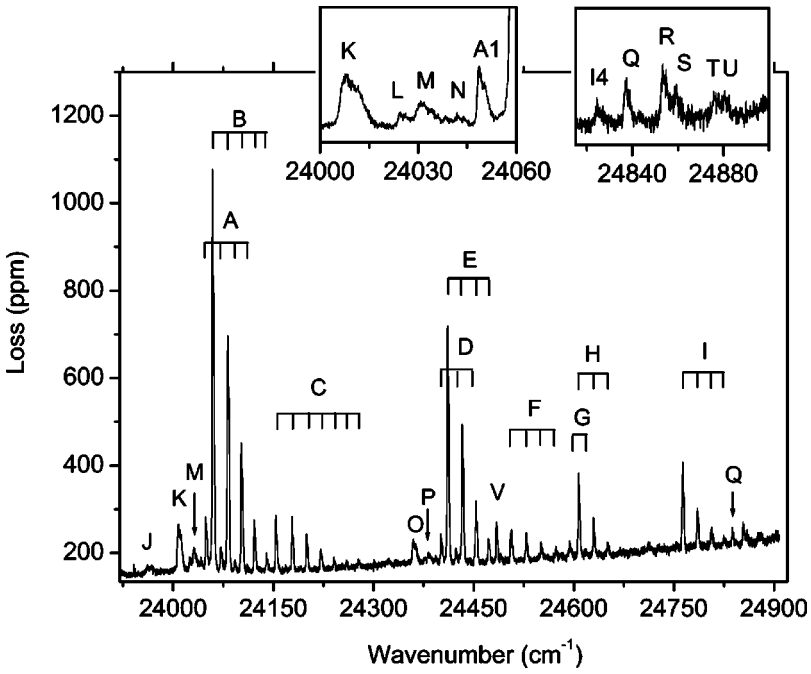

FIG. 1. Cavity ring-down spectrum of perylene. Perylene was heated to 217 °C and prepared in a jet expansion with Ar buffer gas. The spectrum was recorded 4 mm downstream of the PDN slit nozzle. The backing pressure was 1.0×10^5 Pa and the background pressure in the chamber was 10.5 Pa. The inset panels show the weak features observed in the 24 000–24 060 and 24 820–24 900 cm^{-1} spectral ranges. The observed features are labeled alphabetically. Features grouped under the same letter are numbered in the increasing order of energy (the numbers are not shown in the figure).

(PDN). The PDN assembly is based on a design by Saykally and co-workers.[31] It consists of a heated copper sample reservoir and a 10 cm long by 200 μm wide slit, which is sealed from inside by a slit poppet driven by three synchronized pulsed solenoid valves (General Valve Series 9). Two stainless knife-edge electrodes are mounted outside the PDN on each side of the slit. The two electrodes are separated by an even gap of 400 μm and configured as the cathode of a high voltage pulse generator. The PDN assembly itself is configured as the anode. This design enables the generation of atomic and molecular ions and radicals in the jet expansion. In the experiment, the high voltage was applied only for the wavelength calibration, which was achieved by monitoring the Ar^* atomic lines generated in the discharge. Perylene was placed on the bottom of the heated sample reservoir to ensure adequate evaporation. The original poppet design was modified to run at higher temperature by replacing the 10 cm long Viton rubber cord with a Vespel plastic rod (Dupont, SP-22 Grade) and by mounting a water-cooling system on the pulsed solenoid valves. With these modifications, we can achieve a constant operating temperature of 300 °C with the PDN assembly.

The supersonic beam containing perylene and Ar was probed by cavity ring-down spectroscopy. The spectra were probed using frequency-double output of a Nd:YAG (yttrium aluminium garnet) (Quanta-Ray Lab 150 from Spectra-Physics) pumped dye laser (Quanta-Ray PDL-2 from Spectra-Physics). A mixture of dye solution of LDS 821 and LDS 869 (Exciton) were used. The bandwidths were 0.18 cm^{-1} and 0.7 cm^{-1} for the fundamental and doubled output, respectively. The ring-down cavity consists of two high-reflectivity (99.99% at 420 nmin) concave (6 m curvature radius) mirrors (Los Gatos Research) mounted 55 cm apart. The typical ring-down time was 10 μs. The ring-down signal was collected by a photosensor module (H6780-04 from Hamamatsu) and digitized by a 20 MHz 12 bit acquisition board (Adlink, PCI9812). The data were then processed by a PC program and the cavity losses were extracted.

B. Results

Figure 1 presents a cavity ring-down spectrum of perylene in the 24000–24900 cm^{-1} spectral range. The spectrum was recorded 4 mm downstream of the slit nozzle with the PDN assembly maintained at a stable temperature of 217 °C. The backing pressure of Ar was 1.0×10^5 Pa and the background pressure was 10.5 Pa. A number of vibronic bands were observed in this spectral region. The observed bands are labeled alphabetically in Fig. 1. The weak bands in the 24 000–24060 and 24820–24900 cm^{-1} spectral ranges are shown as two insets in Fig. 1. Bands grouped under the same letter are numbered in the increasing order of energy (the numbers are not shown in Fig. 1). A series of bands with similar bandwidths, labeled $A-I$ are predominant in the spectrum. The profiles of these bands are found to be neither Gaussian nor Lorentzian, but rather to be determined by their rotational contour. In addition to these narrow bands, several relatively broader bands, labeled $J-N$, O, and P, were also observed. All these spectral features could not be observed when the PDN assembly was kept at room temperature. When Ar was replaced by He as the carrier gas, the spectrum became very noisy. This is due in part to the much larger leaking rate of He through the modified Vespel plastic poppet (the background pressure increased to 20 Pa for the same backing pressure of 1.0×10^5 Pa). With He as the carrier gas, the strong bands ($B1-B3$, $E1$, $E2$, $H1$, and $I1$) remained essentially the same, while all the weak bands were buried by noise and became indiscernible. Based on these observations, we assign the observed bands (with the exception of J) to perylene. This assignment is further confirmed by the Franck–Condon treatment discussed later in this paper.

We fitted the observed bands with a Gaussian profile.

TABLE I. Band positions, Gaussian widths, intensities, and vibrational assignment for bands in the cavity ring-down spectra of perylene.

Band	Position[a]	Width[a]	Assignment
J	23 966.3(4)	15.2(15)	Complex(?)
K	24 009.5(4)	6.4(4)	$(1a_u)_2^0$
L	24 025.9(4)	5.1(97)	$(1a_u)_3^1(1b_{1u})_1^1$
M	24 031.7(4)	4.4(4)	$(1a_u)_3^1$
N	24 042.5(4)	4.7(22)	$(1b_{1u})_2^2$
*A*1	24 049.5(4)	2.9(3)	$(1b_{1u})_1^1$
*A*2	24 072.2(4)	3.1(3)	$(1a_u)_1^1(1b_{1u})_1^1$
*A*3	24 092.8(4)	3.1(6)	$(1a_u)_2^2(1b_{1u})_1^1$
*B*1	24 059.7(4)	3.1(1)	0_0^0
*B*2	24 082.3(4)	3.1(1)	$(1a_u)_1^1$
*B*3	24 102.9(4)	2.8(2)	$(1a_u)_2^2$
*B*4	24 122.2(4)	2.7(2)	$(1a_u)_3^3$
*B*5	24 140.3(4)	2.9(4)	$(1a_u)_4^4$
*C*1	24 154.3(4)	2.5(2)	$(1a_u)_0^2$
*C*2	24 178.7(4)	2.5(2)	$(1a_u)_1^3$
*C*3	24 200.3(4)	2.6(2)	$(1a_u)_2^4$
*C*4	24 221.6(4)	3.1(3)	$(1a_u)_3^5$
*C*5	24 241.1(4)	3.6(8)	$(1a_u)_4^6$
*C*6	24 259.8(4)	3.2(8)	$(1a_u)_5^7$
*C*7	24 278.1(4)	2.8(5)	$(1a_u)_6^8$
O	24 361.5(4)	6.9(5)	$(1a_u)_2^0(1a_g)_0^1$
P	24 383.2(4)	5.5(9)	$(1a_u)_3^1(1a_g)_0^1$
*D*1	24 401.8(4)	3.1(4)	$(1b_{1u})_1^1(1a_g)_0^1$
*D*2	24 423.8(4)	2.5(3)	$(1a_u)_1^1(1b_{1u})_1^1(1a_g)_0^1$
*D*3	24 444.3(4)	3.5(12)	$(1a_u)_2^2(1b_{1u})_1^1(1a_g)_0^1$
*E*1	24 411.5(4)	2.9(1)	$(1a_g)_0^1$
*E*2	24 433.6(4)	2.8(1)	$(1a_u)_1^1(1a_g)_0^1$
*E*3	24 453.8(4)	2.8(2)	$(1a_u)_2^2(1a_g)_0^1$
*E*4	24 472.9(4)	3.2(3)	$(1a_u)_3^3(1a_g)_0^1$
*E*5	24 491.0(4)	2.9(7)	$(1a_u)_4^4(1a_g)_0^1$
V	24 484.7(4)	2.4(2)	$(2a_g)_0^1$
*F*1	24 506.5(4)	3.1(2)	$(1a_u)_0^2(1a_g)_0^1$
*F*2	24 529.4(4)	2.8(2)	$(1a_u)_1^3(1a_g)_0^1$
*F*3	24 551.4(4)	2.4(2)	$(1a_u)_2^4(1a_g)_0^1$
*F*4	24 573.4(4)	2.4(4)	$(1a_u)_3^5(1a_g)_0^1$
*G*1	24 594.3(4)	2.6(3)	$(1a_u)_4^6(1a_g)_0^1+(1b_{1u})_1^1(3a_g)_0^1$
*H*1	24 607.6(4)	2.6(1)	$(3a_g)_0^1$
*H*2	24 630.1(4)	2.4(1)	$(1a_u)_1^1(3a_g)_0^1$
*H*3	24 650.9(4)	3.1(3)	$(1a_u)_2^2(3a_g)_0^1$
*I*1	24 763.3(4)	2.6(1)	$(1a_g)_0^2$
*I*2	24 785.5(4)	2.8(1)	$(1a_u)_1^1(1a_g)_0^2$
*I*3	24 806.1(4)	2.9(2)	$(1a_u)_2^2(1a_g)_0^2$
*I*4	24 825.5(4)	3.1(6)	$(1a_u)_3^3(1a_g)_0^2$
Q	24 837.5(4)	2.1(2)	$(1a_g)_0^1(2a_g)_0^1$
R	24 853.9(4)	2.6(2)	$(4a_g)_0^1$
S	24 858.9(4)	4.1(6)	$(1a_u)_0^2(1a_g)_0^2+(1a_u)_1^1(1a_g)_0^1(2a_g)_0^1$
T	24 875.8(4)	3.2(9)	$(1a_u)_1^1(4a_g)_0^1$
U	24 880.8(4)	5.5(30)	$(1a_u)_2^2(1a_g)_0^1(2a_g)_0^1$

[a]The values are in units of cm^{-1}.

The fitted positions and widths are listed in Table I. As shown in Table I, the bands grouped under the same letter are separated by a roughly equal spacing. We fitted this spacing with the formula $\Delta\omega_e(v+1/2)-\Delta\omega_e x_e(v+1/2)^2$, and derived $\Delta\omega_e$ to be ca. 23.9 cm^{-1} assuming that $v=0$ for the first band in each of the band systems. The pattern seen in the band systems *K*, *A*, *B*, and *C* is repeated in the similar but weaker band systems *O*, *D*, *E*, and *F* that are shifted to the blue by $\approx$352 cm^{-1}. Several other similar pattern repetitions can be identified as follows: *B* and *H* 548 cm^{-1}, *A* and *G* (548 cm^{-1}), *B* and *I* ($704=2\times352$ cm^{-1}).

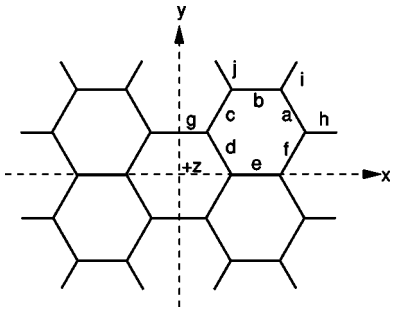

FIG. 2. The coordinate system used in the quantum chemical calculations of perylene. The calculations were performed in the D_{2h} symmetry. Unique bonds in the molecule are labeled alphabetically as a–j.

III. THEORY

To interpret the observed spectrum, we have carried out a rotational contour analysis and a Franck–Condon treatment. Single-excitation configuration-interaction[32] (CIS) calculations were performed to determine the equilibrium geometries, harmonic frequencies, and normal coordinates in both the S_0 and S_1 electronic states. It should be pointed out that the single excitations have no contributions to the S_0 electronic wave function due to the Brillouin theorem, and therefore the CIS calculations are actually the Hartree–Fock (HF) calculations for the S_0 electronic state. Density functional theory[33–35] (DFT) calculations with the Becke's three-parameter exchange functional[36] and the correlation functional of Lee, Yang, and Parr (LYP) (Refs. 37 and 38) were also performed to determine the harmonic frequencies and normal coordinates in the S_0 state. All calculations were carried out with the Gaussian03 code[39] The coordinate system used in the calculations is shown in Fig. 2. The D_{2h} point group was used in the calculations.

A. Rotational contour analysis

The equilibrium geometries in both the S_0 and S_1 electronic states were determined by the CIS calculations with the 6-31G(*d*,*p*) (Refs. 40 and 41) basis set. The vertical transition energy was found to be very sensitive to the polarization functions, especially to the *d* functions on the C atoms. The calculated vertical transition energy is too high without the inclusion of the polarization functions. Table II lists the calculated equilibrium geometries in both states. The calculated geometry in the S_0 state is in good agreement with that determined by x-ray diffraction.[42] The equilibrium rotational constants were determined as $A''=0.0211$ cm^{-1}, $B''=0.0111$ cm^{-1}, $C''=0.007\,27$ cm^{-1} and $A'=0.0208$ cm^{-1}, $B'=0.0113$ cm^{-1}, $C''=0.007\,31$ cm^{-1} in S_0 and S_1, respectively. We have selected the strongest band B_1 in Fig. 1 for a rotational contour analysis because this band has the best S/N ratio and is associated with the 0-0 vibronic transition (as determined in the Franck–Condon treatment). The deviation from the equilibrium rotational constants caused by anharmonicity is therefore expected to be small for this band.

TABLE II. Bond lengths (the unique bonds are labeled in Fig. 2) of perylene (in angstroms).

	S_0 (^1A_g)		S_1 ($^1B_{3u}$)
	HF/6-31G(d,p)	Expt.[a]	CIS/6-31G(d,p)
a	1.356	1.370	1.381
b	1.407	1.418	1.379
c	1.370	1.397	1.416
d	1.430	1.425	1.419
e	1.413	1.424	1.431
f	1.416	1.400	1.406
g	1.486	1.471	1.441
h	1.076		1.076
i	1.076		1.076
j	1.072		1.071

[a]From Ref. 42 and averaged to D_{2h} geometry.

Perylene is an asymmetric top molecule in both the S_0 and S_1 electronic states. The rotational wave function of an asymmetric top molecule can be expressed as J_{K_a,K_c}.[43,44] The asymmetric top rotational wave functions are often grouped in accordance to the parity of the K_aK_c pair: *ee*, *eo*, *oe*, *oo*, where *e* represents even and *o* represents odd. In order to simulate the rotational contour, the nuclear statistical weights for these four types of rotational wave functions need to be determined. We use the method proposed by Landau and Lifshitz[45] and later corrected by Jonas.[46] In this method, the character (denoted by χ^{sw}_{rve}) of an operation P in the molecular symmetry[44] group of the molecule in the representation (denoted by Γ^{sw}_{rve}) spanned by the rovibronic wave functions allowed by the nuclear statistics is given by

$$\chi^{sw}_{rve} = 2\prod (2I_a+1)(-1)^{(2I_a)(n_a-1)}, \tag{1}$$

where the multiplication contains one factor for each group of n_a nuclei having nuclear spin I_a permuted by P. The character is zero if P is a permutation-inversion operation. The reduction of Γ^{sw}_{rve} into the irreducible representations gives rise to the nuclear statistical weights for the corresponding rovibronic wave functions. In the case of perylene with the coordinates shown in Fig. 2, Γ^{sw}_{rve} is reduced as

$$\Gamma^{sw}_{rve} = 1072A_g \oplus 1072A_u \oplus 1008B_{1g} \oplus 1008B_{2g} \oplus 1008B_{3g} \oplus 1008B_{1u} \oplus 1008B_{2u} \oplus 1008B_{3u}. \tag{2}$$

The symmetry species of the *ee*, *eo*, *oe*, *oo* rotational wave functions are deduced by using the asymmetric top symmetry rule.[44] In the case of perylene, the results are $ee-A_g$, $eo-B_{3g}$, $oe-B_{1g}$, and $oo-B_{2g}$. Since the vibronic wave function in the vibrational ground state in the S_0 manifold is totally symmetric ($\Gamma_{ve}=\Gamma_{elec}\otimes\Gamma_{vib}=A_g\otimes A_g=A_g$), the symmetries of the rovibronic wave functions in the S_0 manifold are the same as those of the rotational part. By an inspection of Eq. (2), the nuclear statistical weights for the rovibronic wave functions having the *ee*, *eo*, *oe*, *oo* rotational wave functions are 1072, 1008, 1008, and 1008, respectively.

The simulation of the rotational contour of band B_1 was carried out using the ASYROTWIN computer code developed by Judge and Clouthier.[47] In the simulation, the equilibrium rotational constants determined by the CIS calculations and the derived nuclear statistical weights were used. We expect a Vogit line shape for the rotational lines, as the result of the convolution of the intrinsic Lorentzian lineshape and the Gaussian lineprofile of the probe laser. The linewidth of the probe laser was determined to be 0.7 cm^{-1} (frequency-doubled output) by an inspection of the Ar atomic lines observed when the discharge was turned on. Since the ASROTWIN code does not support Vogit line shape, the simulation was first performed with a Lorentzian line shape and the output was then processed with a small computer code to include the effect of the laser line shape. The simulation was performed by varying the rotational temperature and the intrinsic Lorentzian line width until a good agreement between the simulated and the experimental spectra was achieved. Figure 3 presents the simulated spectrum (dotted line) along with the experimental spectrum (solid line). The agreement between the simulated and experimental spectra is very good. From the simulation, the rotational temperature was determined to be 52 ± 4 K and the intrinsic Lorentzian linewidth was determined to be 0.65 ± 0.05 cm^{-1}.

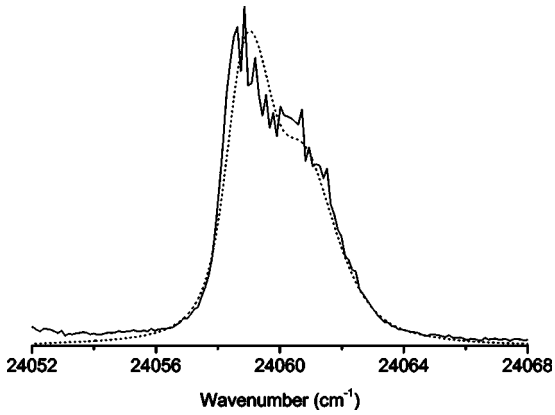

FIG. 3. Simulation of the rotational contour of the strongest band $B1$ of perylene. The solid line represents the experimental spectrum while the dotted line represents the simulated spectrum. The equilibrium rotational constants determined by CIS/6-31G(d,p) were used in the simulation. A Voigt line shape with $\sigma=0.7$ cm^{-1}, as determined by the Ar atomic lines, and $\gamma=0.65$ cm^{-1} was found to well fit the experimental spectrum.

B. Harmonic frequencies and normal coordinates

The harmonic vibrational frequencies and normal coordinates of the 90 normal modes in both the S_0 and S_1 electronic states were determined by the CIS (HF for S_0) calculations with the 6-31G(d,p) basis set. The 6-31++G(d,p) basis set was also used in the frequency calculation of the S_0 state. It has been known that DFT calculations produce more reliable frequencies than the CIS method in which only limited configuration interactions are treated. We therefore also performed a DFT calculation of the S_0 state using the hybrid B3LYP functional with the 6-31++G(d,p) basis set. Care has been taken to ensure strict convergence in light of the existence of several low-frequency modes of perylene.

The 90 calculated harmonic frequencies in both the S_0 and S_1 electronic state using HF/6-31G(d,p), B3LYP/6-31++G(d,p), and CIS/6-31G(d,p) are listed in Table III.

TABLE III. Harmonic frequencies of perylene (in cm^{-1}). The scale factors used in the calculations are 0.91, 0.98, and 0.91 for HF/6-31G(d,p), B3LYP/6-31++G(d,p), and CIS/6-31E(d,p), respectively.

Normal mode	S_0 (^1A_g)			S_1 ($^1B_{3u}$)	
	HF/6-31G(d,p)	B3LYP/6-31++G(d,p)	Expt.	CIS/6-31G(d,p)	Expt.
$1a_u$	5.5(10.8)[a]	23.9	24.5[b], 25.1[c]	36.8[d]	48[b], 47.3[c]
$1b_{1u}$	95.3	93.6	94[b]	86.1	84[b]
$1b_{2g}$	119.3	125.6		137.1[d]	
$2b_{1u}$	176.0	175.5		176.8	
$1b_{3g}$	208.0	203.2		192.1	
$2a_u$	239.3	233.5		226.3	
$1b_{2u}$	247.0	249.1		243.4	
$2b_{2g}$	297.8	294.0		278.1	
$1a_g$	344.6	348.6	353[b]	344.3	351.8[c]
$1b_{1g}$	351.7	358.2		357.3	
$2a_g$	422.3	426.0	427[b]	424.7	425.0[c]
$2b_{3g}$	426.0	420.0		389.2	
$3b_{2g}$	451.1	452.7		481.5	
$1b_{3u}$	454.8	458.8		448.9	
$3b_{1u}$	472.1	473.5		480.8	
$2b_{2u}$	527.3	530.4		507.2	
$2b_{1g}$	528.2	532.7		521.0	
$3a_u$	531.8	525.8		500.6	
$3a_g$	533.8	543.2	547[b]	536.7	547.9[c]
$4b_{1u}$	555.3	549.8		527.5	
$2b_{3u}$	577.2	576.2		557.2	
$3b_{1g}$	615.0	621.5		609.4	
$3b_{3g}$	628.3	622.8		599.9	
$4a_u$	643.8	640.6		628.3	
$4b_{2g}$	655.8	645.4		635.9	
$3b_{2u}$	763.8	767.5		747.0	
$5b_{2g}$	767.2	738.8		718.1	
$4b_{3g}$	774.5	748.3		744.0	
$3b_{3u}$	776.9	785.3	791[e]	784.5	
$5b_{1u}$	780.0	760.1	765, 772[c]	734.0	
$4a_g$	784.6	791.2	801[b]	789.7	797[b], 794.2[c]
$5a_u$	788.3	766.2		758.0	
$4b_{3u}$	807.7	811.7		790.0	
$6b_{1u}$	833.1	806.8	811, 815[e]	783.7	
$6b_{2g}$	852.1	815.7		780.1	
$6a_u$	914.1	877.3		843.2	
$5b_{3g}$	923.7	885.0		864.1	
$7b_{2g}$	930.5	895.9		887.8	
$7b_{1u}$	939.3	904.7		900.9	
$4b_{1g}$	944.2	940.5		936.2	
$5a_g$	966.4	974.0		973.7	
$5b_{1g}$	987.0	1056.5		1054.8	
$7a_u$	1002.5	957.8		978.8	
$6b_{3g}$	1005.1	961.9		985.2	
$8b_{2g}$	1011.2	966.1		986.8	
$8b_{1u}$	1013.5	970.3	969[e]	991.4	
$4b_{2u}$	1019.2	1043.1	1047[e]	986.2	
$5b_{3u}$	1080.4	1092.6	1088, 1089[e]	1090.9	
$6a_g$	1096.3	1106.0	1102[b]	1103.5	1099[b]
$5b_{2u}$	1104.3	1130.1	1131, 1132[e]	1060.0	
$6b_{1g}$	1116.2	1147.2		1115.1	
$6b_{2u}$	1132.1	1190.7		1128.7	
$6b_{3u}$	1149.7	1148.5		1138.0	
$7a_g$	1190.2	1191.4		1194.5	
$7b_{1g}$	1191.6	1193.2		1156.8	
$7b_{2u}$	1191.7	1215.0		1184.8	
$8b_{1g}$	1204.3	1224.3		1210.8	

TABLE III. (*Continued.*)

Normal mode	S_0 (^1A_g)			S_1 ($^1B_{3u}$)	
	HF/6-31G(d,p)	B3LYP/6-31++G(d,p)	Expt.	CIS/6-31G(d,p)	Expt.
$7b_{3u}$	1216.1	1212.5	1216, 1218[e]	1183.9	
$8b_{2u}$	1269.8	1283.2		1299.6	
$8a_g$	1304.9	1298.8	1300[b]	1277.3	1292[b]
$9b_{1g}$	1313.5	1356.6		1300.9	
$9b_{2u}$	1322.9	1336.4		1223.8	
$8b_{3u}$	1335.2	1366.1	1374.5[e]	1221.9	
$9a_g$	1342.7	1364.4		1356.7	
$10a_g$	1368.1	1375.1	1372[b]	1374.7	1398[b]
$9b_{3u}$	1388.4	1384.4	1385[e]	1387.3	
$11a_g$	1449.3	1445.5		1476.2	
$10b_{3u}$	1457.5	1448.1		1444.5	
$10b_{1g}$	1471.3	1460.1		1450.0	
$10b_{2u}$	1496.4	1480.2		1366.2	
$11b_{2u}$	1521.2	1509.6	1500.5[e]	1486.5	
$11b_{1g}$	1533.7	1531.1		1559.3	
$12a_g$	1623.0	1578.0	1580[b]	1622.4	1603[b]
$11b_{3u}$	1627.6	1598.3	1597[e]	1581.5	
$13a_g$	1636.9	1603.6		1557.1	
$12b_{3u}$	1639.6	1604.8		1554.3	
$12b_{2u}$	1653.7	1618.6	1613.5[e]	1568.9	
$12b_{1g}$	1672.1	1632.4		1585.3	
$13b_{1g}$	3039.9	3114.2		3040.8	
$13b_{2u}$	3040.4	3114.6		3041.1	
$13b_{3u}$	3042.6	3116.4		3043.6	
$14a_g$	3043.5	3117.0		3044.2	
$14b_{1g}$	3057.8	3130.0		3057.8	
$14b_{2u}$	3059.8	3132.4		3058.8	
$14b_{3u}$	3060.9	3131.5	3057–3095[e]	3061.0	
$15a_g$	3063.1	3134.1		3062.4	
$15b_{1g}$	3078.2	3146.4		3088.2	
$15b_{3u}$	3078.6	3146.7		3088.2	
$15b_{2u}$	3103.4	3161.7		3115.9	
$16a_g$	3103.4	3161.9		3116.6	

[a]The value in the parentheses was obtained with the HF/6-31++G(d,p) method with a scale factor of 0.91.
[b]From Ref. 26.
[c]This work.
[d]The frequencies of these modes differ by more than 10% between the S_0 and S_1 states.
[e]From Ref. 22.

The scale factors used for the three methods are 0.91, 0.98, and 0.91, respectively. The normal modes are labeled by their symmetries. Modes of the same symmetry are numbered in the order of increasing vibrational frequency in the S_0 state. Care has been taken to best correlate the normal modes in the S_1 state with those in the S_0 state by an inspection of the vibrational mode forms and the reduced masses, and several swaps have been made accordingly. The frequencies in the S_0 state calculated with HF/6-31++G(d,p) were found to be very close to those calculated with HF/6-31G(d,p) except for the lowest $1a_u$ mode. The frequencies of this mode calculated with HF/6-31G(d,p), HF/6-31++G(d,p), and B3LYP/6-31++G(d,p) are 5.5 cm^{-1}, 10.8 cm^{-1}, and 23.9 cm^{-1}, respectively, indicating that the frequency calculations for very-low-frequency modes are very sensitive to diffuse functions and electron correlation. The frequencies of this $1a_u$ mode in the S_0 and S_1 states have been determined by laser-induced experiment to be 24.5 and 48 cm^{-1}, respectively.[26] Except for this mode, the HF/6-31G(d,p) predicts values very close to those predicted with B3LYP/6-31++G(d,p) at low frequencies but begins to systematically underestimate the values at high frequencies (>3000 cm^{-1}).

Ohno and co-workers[48,49] have shown that conventional quantum chemical methods might fail to predict a reliable harmonic frequency for a normal mode in an electronically excited aromatic molecule if there exist a strong vibronic coupling between this mode and another mode in a nearby electronic state. In such a case, dramatic frequency upshift (coupling with a lower vibronic state) or downshift (coupling with a higher vibronic state) and change of vibrational mode form (Duschinsky effect[50]) can be observed for this mode. An inspection of the frequencies calculated with HF/6-31G(d,p) and CIS/6-31G(d,p) shows only two modes whose frequencies differ by more than 10% between the S_0

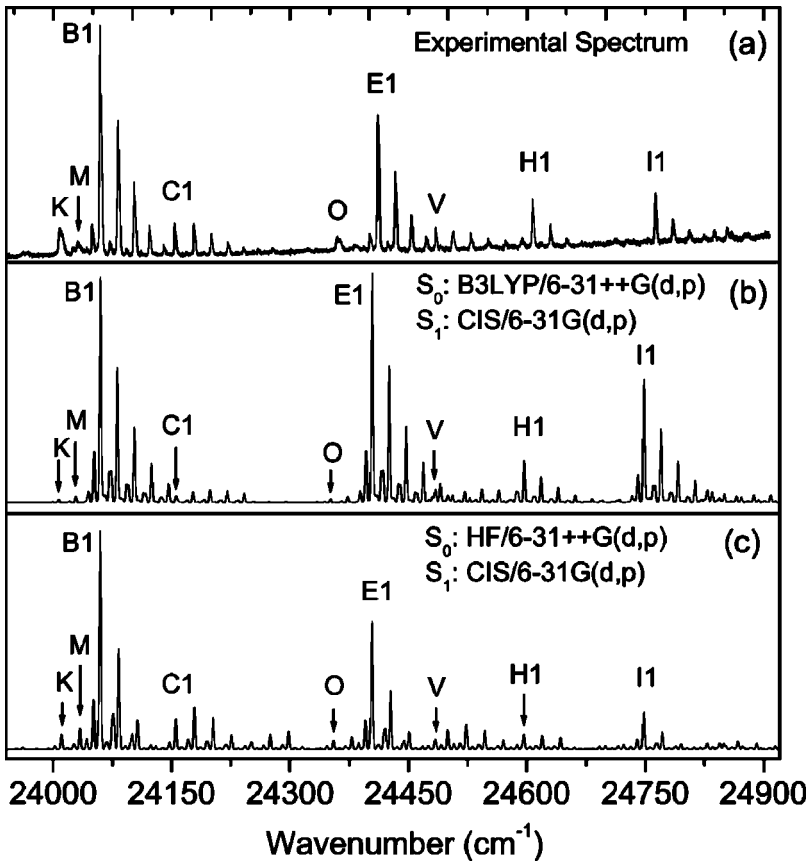

FIG. 4. Comparison of the calculated and experimental spectra. The calculated spectra are convoluted with a Gaussian function of $\sigma=2.5\ \mathrm{cm}^{-1}$ and are shifted so that band $B1$ falls at the experimentally measured position. Several major spectral features are labeled in the same way as in Fig. 1. (a) The experimental spectrum. (b) The spectrum calculated using the normal coordinates calculated with B3LYP/6-31++G(d,p) and CIS/6-31G(d,p) in the S_0 and S_1 electronic states, respectively. (c) The spectrum calculated using the normal coordinates calculated with HF/6-31++G(d,p) and CIS/6-31G(d,p) in the S_0 and S_1 electronic states, respectively.

and S_1 state: $1a_u$ and $1b_{2g}$. These two modes are labeled "d" in Table III to indicate possible inaccuracy of the calculated frequencies in the S_1 state.

C. Franck–Condon treatment and vibrational assignment

A Franck–Condon treatment has been carried out to calculate the observed vibronic spectrum. In this treatment, a set of normal modes was selected and the vibrational quanta in these modes in the S_0 and S_1 electronic states were specified. The Franck–Condon factors between the vibrational states generated this way in the S_0 and S_1 electronic states were then evaluated using the normal coordinates obtained in the frequency calculations. The evaluation of the Franck–Condon factors was performed using the MOLFC computer code developed by Borrelli and co-workers.[51] The vibronic spectrum is then calculated using the obtained Franck–Condon factors and by assuming a same vibrational temperature for all the normal modes selected. In this Franck–Condon treatment, we effectively ignored the dependence of the electronic transition dipole moment on the nuclear coordinates of the molecule. This should be a good approximation if the vibrational excitation in the molecule is low since in such a case, the vibrational wave functions are mainly localized in the vicinity of the equilibrium geometry of the S_0 state.

Two calculated vibronic spectra of the $S_1 \leftarrow S_0$ transition of perylene are presented in Fig. 4. The experimental spectrum is presented in Fig. 4(a). The spectrum presented in Fig. 4(b) was calculated using the normal coordinates calculated with B3LYP/6-31++G(d,p) and CIS/6-31G(d,p) in the S_0 and S_1 electronic states, respectively, while the spectrum presented in Fig. 4(c) was calculated using the normal coordinates calculated with HF/6-31++G(d,p) and CIS/6-31G(d,p) in the S_0 and S_1 electronic states, respectively. The calculated spectra are convoluted with a Gaussian function of $\sigma=2.5\ \mathrm{cm}^{-1}$ and are shifted so that band B_1 falls at the experimentally measured position. Several major spectral features are labeled in all the spectra in the same way as in Fig. 1 to assist in the correlation of the calculated features with the experimental features. In the calculations of the vibronic spectra, six normal modes were selected: $1a_u$, $1b_{1u}$, $1a_g$, $2a_g$, $3a_g$, and $4a_g$. A vibrational temperature of 90 K was used in the calculations for the purposes of "magnifying" weak hot bands. As discussed in the previous section, the frequencies of the $1a_u$ mode calculated with the HF and CIS methods are not reliable. Since this mode is expected to have significant excitations because of its very low frequency in the S_0 state, we used the experimental frequencies[26] for this mode after the Franck–Condon calculations to generate reliable positions for the spectral features associated with this mode. As shown in Fig. 4, the two calculated vibronic spectra are in very good agreement with the experimental spectrum. In general, the calculated spectrum shown in Fig. 4(b) matches better with the experimental spectrum than the calculated spectrum shown in Fig. 4(c). The intensities of bands $B2$ [transition $(1a_u)_1^1$]-$B5$ [transition $(1a_u)_4^4$], $H1$ [transition $(3a_g)_0^1$]-$H3$ [transition $(1a_u)_2^2(3a_g)_0^1$], and $E2$ [transition $(1a_u)_1^1(1a_g)_0^1$]-$E4$ [transition $(1a_u)_3^3(1a_g)_0^1$] in the calculated spectrum shown in Fig. 4(b) are in better

agreement with the experimental intensities than those of the corresponding bands in the spectrum shown in Fig. 4(c), while the intensities of bands *K* [transition $(1a_u)_2^0$], *L* [transition $(1a_u)_3^1(1b_{1u})_1^1$], *M* [transition $(1a_u)_3^1$], *N* [transition $(1b_{1u})_2^2$], *O* [transition $(1a_u)_2^0(1a_g)_0^1$], *C*1 [transition $(1a_u)_0^2$]-*C*4 [transition $(1a_u)_3^5$], and *R* [transition $(4a_g)_0^1$] in the calculated spectrum shown in Fig. 4(c) are in better agreement with the experimental intensities than those of the corresponding bands in the spectrum shown in Fig. 4(b).

With the help of these two calculated vibronic spectra, the observed spectral features except *J* can be positively assigned. This assignment is listed in Table I along with the fitted band positions and widths. From the vibrational assignment, the frequencies of mode $1a_u$ in the S_0 and S_1 states are determined to be 25.1 cm^{-1} and 47.3 cm^{-1} using the positions of bands *K* [transition $(1a_u)_2^0$] and *C*1 [transition $(1a_u)_0^2$], respectively. The frequencies of modes $1a_g$, $2a_g$, $3a_g$, and $4a_g$ in the S_1 state are determined to be 351.8 cm^{-1}, 425.0 cm^{-1}, 547.9 cm^{-1}, and 794.2 cm^{-1} using the positions of bands *E*1 [transition $(1a_g)_0^1$], *V* [transition $(2a_g)_0^1$], *H*1 [transition $(3a_g)_0^1$], and *R* [transition $(4a_g)_0^1$], respectively. The frequency difference of mode $1b_{1u}$ between the S_0 and S_1 states is determined to be -10.2 cm^{-1} by using the spacing between bands *A*1 [transition $(1b_{1u})_1^1$] and B_1 (transition 0-0). These experimentally derived frequencies are listed in Table III. We also list in Table III the frequencies derived from other experimental data[22,26] that can be correlated to our calculated normal modes. Bands *K*, *L*, *M*, *N*, *O* and *P* (in particular *K* and *O*) are broader than the other features. This could be attributed to nearby unidentified hot-band transitions. No reasonable assignment can be made for band *J* from our Franck–Condon treatment. We suspect that this feature is due to the transition of van der Waals complex formed between perylene and Ar in the expanding jet.

IV. DISCUSSION

In this paper, we have presented the cavity ring-down spectrum and quantum chemical calculations of the $S_1 \leftarrow S_0$ transition of perylene. Most vibronic bands were assigned in the Franck–Condon treatment. The vibronic spectra calculated in the Franck–Condon treatment are found to be in very good agreement with the experimental spectrum. As shown in Table III, the calculated frequencies are in very good agreement with the experimental frequencies derived from this work and from other experimental work.[22,26] This is particularly true for the frequencies in the S_0 state predicted with B3LYP/6-31++G(d,p). One relatively large disagreement is found for the frequencies of mode $1a_u$ predicted with HF and CIS, indicative of the sensitivity of the frequency calculation of very-low-frequency modes to the diffuse functions and electronic correlation. One conclusion of the present paper is the necessity, in the frequency calculation for very-low-frequency modes of polycyclic aromatic molecules, of inclusion of diffuse functions and electron correlation.

The good agreement observed between the calculated and experimental frequencies is partly attributed to the large energy gaps between S_0 and S_1 (2.98 eV), and between S_1 and S_2 ($\sim$0.82 eV). Large energy gaps result in weak vibronic interactions between the electronic states. As shown in this work, the harmonic approximation works very well for perylene. This is not surprising if one considers the fact that perylene is a compact and therefore relatively rigid structure. This point is very well illustrated with a comparison of perylene with pentacene that has a linear and therefore relatively floppy structure. It has been shown[52,53] that pentacene has a very anharmonic "butterfly" mode $(1b_{1u})$ with a theoretical frequency of ca. 42 cm^{-1} in the S_0 state. The 2-0, 4-0, and 6-0 vibronic transitions in this mode form the strong features observed in the $S_1 \leftarrow S_0$ transition of pentacene at 81, 195, 332, and 342 cm^{-1}, respectively. It also has been shown that pentacene is quasiplanar in the S_1 state. We have employed the same Franck–Condon treatment to pentacene and completely failed to predict the strong 2-0, 4-0, and 6-0 vibrational transitions in the $1b_{1u}$ mode. The frequency of the butterfly mode is usually a measure of the rigidity of an aromatic molecule. Compared to pentacene, the butterfly mode $(1b_{1u})$ in perylene has a frequency of ca. 94 cm^{-1}, indicating that perylene is more rigid than pentacene.

It is interesting to compare our results with earlier LIF experiments. In two papers published by Tramer and coworkers, the fluorescence excitation and dispersion spectra of the same transition were recorded to study the IVR of perylene.[25,26] Although the fluorescence excitation spectrum was not published in these papers, the authors reported that the strongest band of the transition was located at 24070 cm^{-1}. This value is 10.3 cm^{-1} to the blue of the strongest band *B*1 observed in our CRDS experiment. We believe that there was probably a wavelength calibration error in these earlier experiments. A number of vibrational frequencies were identified in their experiments. We could match the reported modes *A*–*G*, *R*, and *S* (Table 2 of Ref. 26) with modes identified or calculated in this work. We have difficulties in identifying other modes reported by these authors. Based on our experiment and theoretical calculations, we believe that mode *H* (20 cm^{-1} in S_0 and 13 cm^{-1} in S_1) does not exist. It is also very likely that only one of modes *J*, *J'* and *K* is real, which can be correlated with mode $1b_{2g}$. In another LIF experiment by Schwartz and co-workers,[27] a frequency of 95 cm^{-1} (Table 1 of Ref. 27) was reported in the S_1 state. We now know from our Franck–Condon treatment that this frequency is not a fundamental frequency of a normal mode but is due to the overtone transition $(1a_u)_0^2$.

For low rovibronic states ($E'_{vib} < 850$ cm^{-1}) in the S_1 manifold of perylene, we expect the lifetimes are determined mainly by the resonant radiation due to the lack of IVR (Refs. 25–27) and the absence of other singlet electronic states in between. This is confirmed by our observation that all vibronic features of perylene have about the same widths (2.4–3.5 cm^{-1}). Middle-size compact neutral PAHs of similar structures as perylene are characterized by well-separated S_0 and S_1 states and a strong transition between the two states with similar oscillator strength.[23] We expect the observed bandwidths of perylene to be typical for these compact neutral PAHs. It has been recognized that small and middle compact PAHs might be present in the interstellar medium as neutral molecules and ions due to strong radiation from nearby stars.[4] The contribution of neutral PAHs and

PAH ions to the DIBs is therefore of great interest. It is interesting to note that more than 50% of the observed DIB features have bandwidths between 2 and 5 cm^{-1}, which cannot be attributed to PAH ions because of their short lifetimes ($\sim$0.2 ps) and broader bandwidths (20–30 cm^{-1}).[15,17,54] We conclude from this study that neutral PAHs are probably more important for these narrow DIB features.

ACKNOWLEDGMENTS

This research was performed while X.T. held a National Research Council Research Associateship Award at NASA Ames Research Center. The authors acknowledge the discussion of nuclear statistics with Dr. Paul J. Dagdigian. The authors are grateful to Dr. Charles W. Bauschlicher for letting them use the GAUSSIAN03 code. The authors also want to thank Robert Walker for excellent technical support. This research was supported by NASA's Science Mission Directorate (APRA program, RTOP No. 188-01-03-01).

[1] *The Diffuse Interstellar Bands*, edited by A. G. G. M. Tielens and T. P. Snow (Kluwer Academic, Dordrecht, Netherlands, 1995).
[2] G. P. van der Zwet and L. J. Allamandola, Astron. Astrophys. **146**, 76 (1985).
[3] A. Léger and L. B. d'Hendecourt, Astron. Astrophys. **146**, 81 (1985).
[4] F. Salama, E. L. O. Bakes, L. J. Allamandola, and A. G. G. M. Tielens, Astrophys. J. **458**, 621 (1996).
[5] G. H. Herbig, Annu. Rev. Astron. Astrophys. **33**, 19 (1995).
[6] S. O. Tuairisg, J. Cami, B. H. Foing, P. Sonnentrucker, and P. Ehrenfreund, Astron. Astrophys., Suppl. Ser. **142**, 225 (2000).
[7] M. C. Heger, Lick Obs. Bull. **10**, 146 (1922).
[8] F. Salama, *The ISO Revolution* (EDP Sciences, Les Ulis, France, 1999), p. 65.
[9] F. Salama and L. J. Allamandola, J. Chem. Phys. **94**, 6964 (1991).
[10] F. Salama, C. Joblin, and L. J. Allamandola, J. Chem. Phys. **101**, 10252 (1994).
[11] G. Berden, R. Peeters, and G. Meijer, Int. Rev. Phys. Chem. **19**, 565 (2000).
[12] J. M. Herbelin, J. A. Mckay, M. A. Kwok, R. H. Ueunten, D. S. Urevig, D. J. Spencer, and D. J. Benard, Appl. Opt. **19**, 144 (1980).
[13] A. O'Keefe and D. A. G. Deacon, Rev. Sci. Instrum. **59**, 2544 (1988).
[14] D. Romanini, L. Biennier, F. Salama, A. Kachanov, L. J. Allamandola, and F. Stoeckel, Chem. Phys. Lett. **303**, 165 (1999).
[15] L. Biennier, F. Salama, L. J. Allamandola, and J. J. Scherer, J. Chem. Phys. **118**, 7863 (2003).
[16] L. Biennier, F. Salama, M. Gupta, and A. O'Keefe, Chem. Phys. Lett. **387**, 287 (2004).
[17] O. Sukhorukov, A. Staicu, E. Diegel, G. Rouillé, T. Henning, and F. Huisken, Chem. Phys. Lett. **386**, 259 (2004).
[18] G. Rouillé, S. Krasnokutski, F. Huisken, T. Henning, O. Sukhorukov, and A. Staicu, J. Chem. Phys. **120**, 6028 (2004).
[19] E. V. Shpol'skii and R. I. Personov, Opt. Spectrosc. **8**, 172 (1960).
[20] T. Tamm and P. Saari, Chem. Phys. **40**, 311 (1979).
[21] I. Abram, R. A. Auerbach, R. R. Birge, B. E. Kohler, and J. M. Stevenson, J. Chem. Phys. **63**, 2473 (1975).
[22] J. Szczepanski, C. Chapo, and M. Vala, Chem. Phys. Lett. **205**, 434 (1993).
[23] T. M. Halasinski, J. L. Weisman, R. Ruiterkamp, T. J. Lee, F. Salama, and M. Head-Gordon, J. Phys. Chem. A **107**, 3660 (2003).
[24] C. Joblin, F. Salama, and L. Allamandola, J. Chem. Phys. **110**, 7287 (1999).
[25] C. Bouzou, C. Jouvet, J. B. Leblond, Ph. Millie, and A. Tramer, Chem. Phys. Lett. **97**, 161 (1983).
[26] B. Fourmann, C. Jouvet, and A. Tramer, Chem. Phys. **92**, 25 (1985).
[27] S. A. Schwartz and M. R. Topp, Chem. Phys. **86**, 245 (1984).
[28] J. C. Whitmer, S. J. Cyvin, and B. N. Cyvin, Z. Naturforsch. **33**, 45 (1978).
[29] M. A. Kovner, A. A. Terekhov, and L. M. Babkov, Opt. Spectrosc. **34**, 615 (1973).
[30] S. R. Langhoff, J. Phys. Chem. **100**, 2819 (1996).
[31] K. Liu, R. S. Fellers, M. R. Viant, R. P. Mclaughlin, M. Brown, and R. Saykally, Rev. Sci. Instrum. **67**, 410 (1996).
[32] J. B. Foresman, M. Head-Gordon, J. A. Pople, and M. J. Frisch, J. Phys. Chem. **96**, 135 (1992).
[33] P. Hohenberg and W. Kohn, Phys. Rev. B **864**, 136 (1964).
[34] W. Kohn and L. J. Sham, Phys. Rev. **140**, A1133 (1965).
[35] R. G. Parr and W. Yang, *Density-Functional Theory of Atoms and Molecules* (Oxford University Press, Oxford, 1989).
[36] A. D. Becke, J. Chem. Phys. **98**, 5648 (1993).
[37] C. Lee, W. Yang, and R. G. Parr, Phys. Rev. B **37**, 785 (1988).
[38] B. Miehlich, A. Savin, H. Stoll, and H. Preuss, Chem. Phys. Lett. **157**, 200 (1989).
[39] M. J. Frisch, G. W. Trucks, H. B. Schlegel *et al.*, GAUSSIAN 03, revision B.05, Gaussian, Inc., Pittsburgh, PA, 2003.
[40] P. C. Hariharan and J. A. Pople, Theor. Chim. Acta **28**, 213 (1973).
[41] P. C. Hariharan and J. A. Pople, Mol. Phys. **27**, 209 (1974).
[42] A. Camerman and J. Trotter, Proc. R. Soc. London, Ser. A **279**, 129 (1964).
[43] R. N. Zare, *Angular Momentum: Understanding Spatial Aspects in Chemistry and Physics* (Wiley, New York, 1988).
[44] P. R. Bunker, P. Jensen, *Molecular Symmetry and Spectroscopy*, 2nd ed. (NRC Research, Ottawa, 1998).
[45] L. D. Landau and E. M. Lifschitz, *Quantum Mechanics*, 3rd ed. (Pergamon, New York, 1977).
[46] D. M. Jonas, J. Chem. Phys. **90**, 5563 (1989).
[47] R. H. Judge and D. J. Clouthier, Comput. Phys. Commun. **135**, 293 (2001).
[48] K. Ohno, Chem. Phys. Lett. **64**, 560 (1979).
[49] K. Ohno and R. Takahashi, Chem. Phys. Lett. **356**, 409 (2002).
[50] F. Duschinsky, Acta Physicochim. URSS **7**, 551 (1937).
[51] R. Borrelli and A. Peluso, J. Chem. Phys. **119**, 8437 (2003).
[52] A. Amirav, U. Even, and J. Jortner, Chem. Phys. Lett. **72**, 21 (1980).
[53] A. M. Griffiths and P. A. Freedman, J. Chem. Soc., Faraday Trans. 2 **78**, 391 (1982).
[54] L. Zhao, R. Lian, I. A. Shkrob, R. A. Crowell, S. Pommeret, E. L. Chronoster, A. D. Liu, and A. D. Trifunac, J. Phys. Chem. A **108**, 25 (2004).